SSC17-XII-05

Brane Craft: Phase I Results

Siegfried W. Janson
The Aerospace Corporation
Mail Stop M2/241, P.O. Box 92957, Los Angeles, CA 90009-2957; Phone: 310.379.7060
siegfried.w.janson@aero.org

ABSTRACT

A Brane Craft is a membrane spacecraft with solar cells, command and control electronics, communications systems, antennas, propulsion systems, attitude and proximity sensors, and shape control actuators as thin film structures manufactured on ~10 micron thick plastic sheets. It enables new missions that require low-mass spacecraft with exceptionally high delta-V such as active removal of orbital debris from Earth orbit (LEO).

An 80-gram mass Brane Craft deployed by the International Space Station could deorbit a debris object of at least 0.9 kg mass in a 2000 km altitude circular orbit with an inclination between 5° and 105°. Two to three weeks is needed to retrieve a debris object anywhere in LEO, once the Right Ascension of the Ascending Nodes (RAANs) of the initial and target orbits line up. Significantly more mass can be retrieved from lower orbits.

Thin-film solar cells and electronics will receive up to 10 megarads total integrated dose (TID) during a nominal 3-week long mission. Thin film Copper Indium Gallium Selenide (CIGS) solar cells and thin film carbon nanotube and ZnO transistors have the required TID radiation tolerance. In addition, particle flux and penetration analyses showed that the propellant storage structure in a Brane Craft could be penetrated up to 30 times over a nominal mission. Nevertheless, the concept appears to be feasible, and could be implemented within a decade.

INTRODUCTION

The Brane Craft was one of 16 efforts selected for Phase I funding during 2016 by NASA's Innovative Advanced Concepts (NIAC) group. "Brane" is short-hand for "membrane," and this radically new spacecraft design enables ultra-light, highly-maneuverable spacecraft that can be mass-produced in 1000+ unit quantities for challenging applications such as orbital debris removal and asteroid inspection. The current design is one meter square with a thickness of 50 microns, and weighs 82 grams with propellant. It has a delta-V of 16 km/s using distributed nano-electrospray thrusters, and due to the extremely high power-to-weight ratio, a maximum acceleration of 0.1 m/s^2. The Phase I effort was a concept study focused on removing orbital debris from low Earth orbit (LEO), and a Phase II technology development effort was recently awarded by NIAC.

HISTORY

More than a decade ago, a colleague of mine noted that the kilogram-class silicon satellite, that I had been promoting for many years, could be used to rendezvous with a piece of orbital debris and actively deorbit it by thrusting against the velocity vector. This was in response to a negative comment made by the late science fiction writer and space visionary Arthur C. Clarke in a letter to Aerospace America in 1996. I proposed LEO constellations of thousands of small satellites in a previous issue, and he was concerned about how to manage the increasing density of orbital objects. My colleague and I developed a catchy acronym called Space DOGS (Disposable Orbital Garbage Sweeper) for the overall mission to individually "fetch" space debris objects and bring them down to a high-drag disposal altitude. Unfortunately, lack of interest and unfavorable economics prevented this idea from catching on.

After decades of more and more satellites being launched into LEO, several satellite-satellite collisions, and a Chinese anti-satellite test, interest in orbital debris reduction has become a national and international concern.

Relatively easy measures to limit the growth of orbital objects and debris include mandating a 25-year maximum orbital lifetime after the mission ends, minimizing the number of free-flying deployed objects

from a spacecraft, and requiring end-of-mission reduction of stored internal energy such as emptying propellant tanks, draining batteries, and disabling solar charging. Active removal of orbital debris is much more difficult because it requires funding and launching a retrieval spacecraft.

SPACE DEBRIS AND OTHER OBJECTS

"The simple definition of space debris is any human-made object in orbit that is not in active use." [1] The lower limit for reliable tracking of an object is 5 to 10 cm, and more than 17,000 objects are tracked by the Space Surveillance Network (SSN). Figure 1 shows the monthly number of all objects officially tracked by the SSN through February, 2016. Big spikes at the end of 2006 and the beginning of 2009 are due to the fragmentation debris from a Chinese anti-satellite test, and a collision between an Iridium satellite (number 33) and Cosmos 2251. Note that it could take a decade for the tracked fragmentation debris level to return to the pre-collision level, assuming no more inadvertent satellite collisions, explosions, or anti-satellite tests.

If ground tracking systems were improved to see down to 1 cm; approximately 500,000 debris objects would fill the catalog. The 2009 Cosmos-Iridium collision generated about 2000 tracked debris objects, over 8000 (estimated) debris objects of size between 3 and 10 cm, and over 150,000 debris objects (estimated) smaller than 3 cm in size.[2] While these may seem physically small, they are still large enough to cause catastrophic damage to an active satellite. Table 1 shows mass, kinetic energy, and equivalent dynamite mass (in sticks) for ideal aluminum spheres colliding with an object at 10 km/s. A 0.5-cm diameter object has the explosive equivalent of 1/113 of a stick of dynamite, roughly equivalent to the impact energy of ten 357 magnum rounds. Ideally, we would like to remove all debris objects larger than this size. However, we only track objects of 5-cm size and larger; about 10,000 debris objects that we can go after in the near future.

Table 1. Mass, kinetic energy, and explosive equivalent in sticks of dynamite for an aluminum sphere colliding with a satellite at 10 km/s.

Debris Diameter	Mass (grams)	Kinetic Energy	Explosive Equivalent
Debris Diameter	Mass (grams)	Kinetic Energy	Explosive Equivalent
0.5 cm	0.177 grams	8.84 kJ	1/113 sticks
1 cm	1.41 grams	70.7 kJ	1/14 stick
3 cm	38.2 grams	1.91 MJ	1.9 sticks
5 cm	177 grams	8.84 MJ	8.8 sticks
10 cm	1.41 kg	70.7 MJ	71 sticks

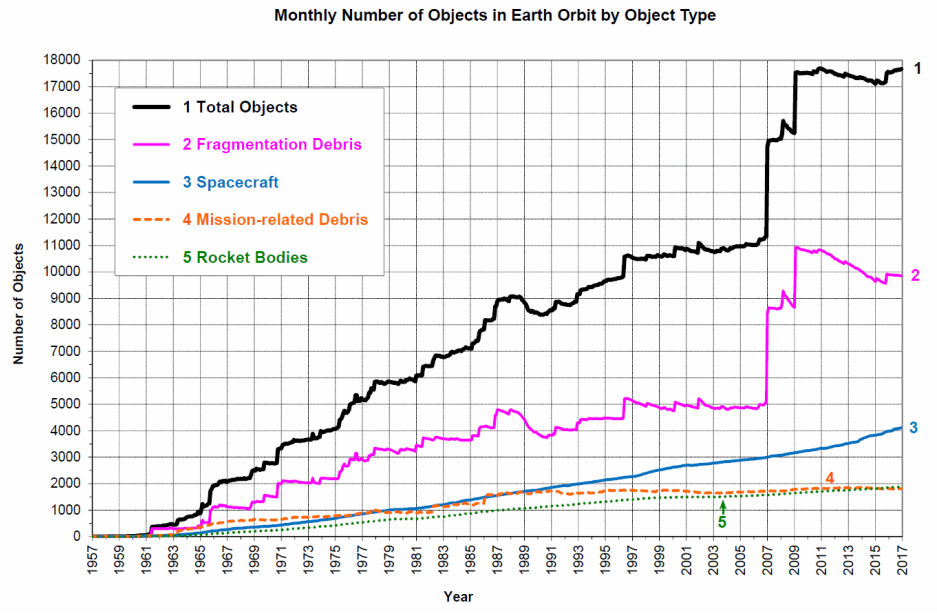

Figure 1. Monthly number of objects tracked by the U.S. Space Surveillance Network. Image, courtesy of NASA, from reference 3.

Where are the majority of orbital debris objects? Figure 2 shows the density of tracked debris objects as a function of altitude in Earth orbit. Highest densities occur in LEO; altitudes between 300 and 2000 km. Note that the highest density is 4 x 10^{-8} objects per cubic kilometer, or one object for every 25 million cubic kilometers. That's about 360 km between nearest neighbors, on average. The next largest density peak occurs in Medium Earth Orbit (MEO), and is primarily due to the U.S. Global Positioning Satellites (GPS) and their international cousins. A larger peak occurs at Geosynchronous Earth Orbit (GEO) where communications and high-altitude weather satellites are relatively stationary above a point on the equator. This is prime satellite real estate.

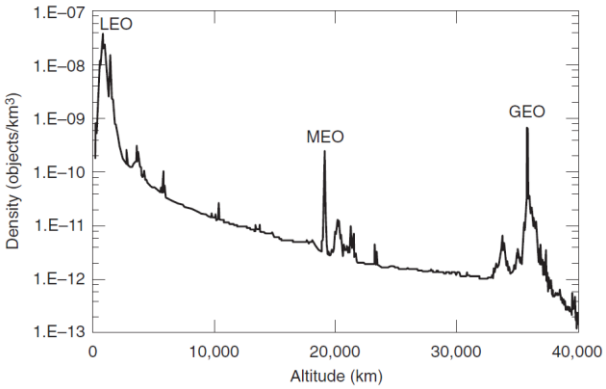

Figure 2. Density of orbital objects as a function of altitude. Image, courtesy of The Aerospace Corporation, from reference 4.

OBJECTS IN LEO

Figure 3 shows density vs. altitude in LEO altitude range using a linear vertical scale. These plots were made in 2007 after the Chinese anti-satellite test that caused the destruction of the Feng Yung 1C (FY1C) weather satellite. Several peaks occur for LEO communications and navigation satellite constellations; Iridium, Orbcomm, Globalstar, Parus, and Strela. The latter two were initiated by the former Soviet Union in the 1970's. Satellite orbits at altitudes above 1000 km are more affected by solar radiation pressure than by atmospheric drag, and can stay in orbit for centuries. Figure 3 shows that orbital debris density (the "Non-satellites" curve) peaks in the 800 to 1000-km range, and drops off by 1800 km.

What is the distribution of orbit inclinations for objects in LEO? Figure 4 shows the distribution of tracked objects in LEO as a function of orbit inclination. The largest population occurs at sun-synchronous inclination which can range from 96.5° to 116°,

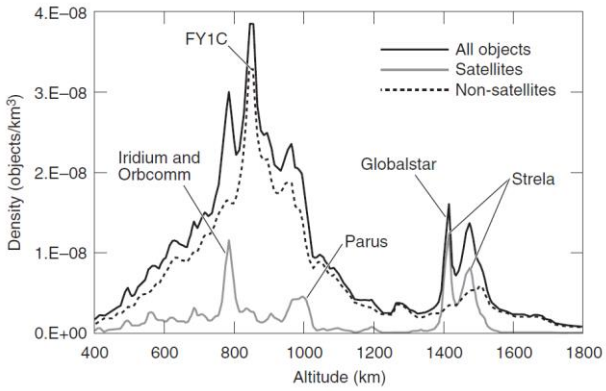

Figure 3. Density of orbital objects as a function of altitude in LEO. Image, courtesy of The Aerospace Corporation, from reference 4.

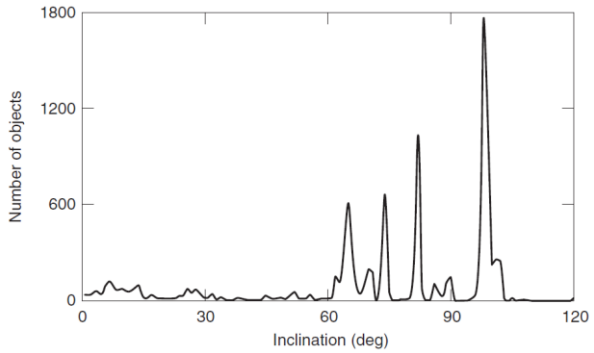

Figure 4. Inclination distribution of objects in low Earth orbit. Image, courtesy of The Aerospace Corporation, from reference 4.

depending on altitude. Note that the vast majority of objects are in orbit inclinations greater than 60°.

THE BRANE CRAFT DESIGN

A Brane Craft is a membrane spacecraft with solar cells, electronics, propulsion, sensors, antennas, actuators, etc., as thin film structures manufactured on plastic sheets. This essentially two-dimensional design can have a thickness of tens of microns with a surface area of square meters. This is a revolutionary spacecraft design that maximizes area-to-mass ratio to enable exceptionally low-mass spacecraft for aperture-driven applications such as communications satellites, solar power satellites, solar electric propulsion stages, and solar sails. It also enables new missions that require thousands of low-mass spacecraft that can significantly change trajectory or orbit. Active removal of orbital debris from Earth orbit was the target application for this study. Figure 5 shows an artist's concept of a 1 square meter Brane Craft about to envelop a piece of space debris in low Earth orbit (LEO).

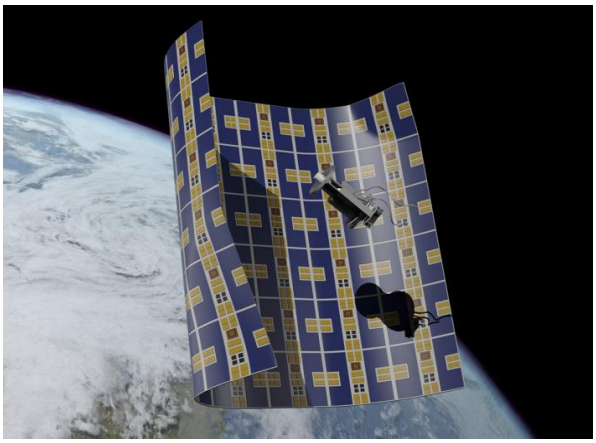

Figure 5. Artist's concept of a Brane Craft in low Earth orbit about to envelop a piece of space debris.

The basic Brane Craft design has distributed arrays of nano-electrospray thrusters that use an ionic liquid propellant. About 1 cm^2 of electrospray thruster area is required to process the 180 W of DC power for propulsion generated by thin film solar arrays deposited over most of the 1-square meter surface. Ionic liquids have essentially zero vapor pressure, and the propellant is stored in the ~10-micron gap between two sheets of Kapton®. Figure 6 shows a schematic cross section of the current design. This Brane Craft design can generate a total of 8.2 millinewtons of thrust at 4000 s specific impulse under full sunlight at 1 astronomical unit (A.U.) from the sun. At 81-grams mass, Brane Craft can accelerate at up to 0.10 m/s^2; at least 100 times faster than a conventional electrically-propelled spacecraft. The 1-square meter design held 27 grams of propellant and generated a total delta-V of 16 km/s at 4000 s specific impulse over 36 hours of thrusting. This is more than enough delta-V to start in a 400-km altitude LEO orbit, maneuver out to a piece of space debris in Low Earth Orbit (LEO), and drag it down to a disposal orbit. If the debris mass was less than ~2 kg in LEO altitudes below 1000-km, the process could be repeated one or more times. If the debris mass were much larger, the object could be deorbited using multiple Brane Craft, sequentially.

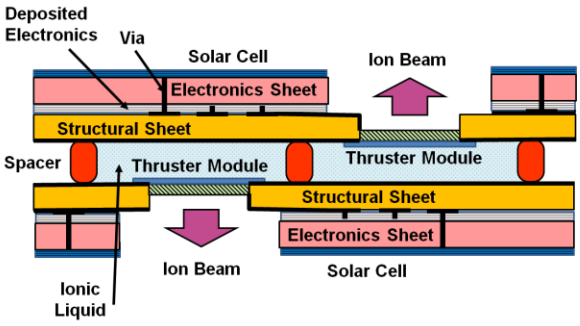

Figure 6. Schematic cross section of a Brane Craft.

The manufacture of thin film solar cells, electronics, sensors, and actuators require different processing steps, some of which occur in vacuum. After studying the types of equipment needed to produce 1 to 10-micron resolution features for Brane Craft electronics, it seemed prudent to print or deposit electronics on 30 cm x 30 cm or smaller substrates rather than the 100 cm by 100 cm substrates used for the primary structure. The 1 square meter sheets were still needed to hold the propellant and thruster modules, but they could also act as a circuit board to electrically connect smaller Kapton® sheets with specific functions. Figure 6 shows two 1-meter square main structural sheets of 10-micron thick Kapton® separated, by a 15-micron high gap that holds the ionic liquid propellant, plus additional 10-micron thick electronics sheets bonded to them. This design provides 7 microns of radiation shielding for the thin film electronics, and also allows replacement and upgradeability of specific spacecraft functions over time by bonding on different electronics sheets.

Solar Cells

Last year, thin film solar cells represented about 7% of global solar cell production in terms of power generation capability (4.2 GW out of 63 GW).[5] Thin film solar cells can have a thickness less than 10 microns, and are thus extremely suitable for integration into active membrane spacecraft. Thin film Cadmium Telluride (CdTe) and Copper Indium Gallium Selenide (CIGS) solar cells on flexible substrates for terrestrial applications are commercially-available from Global Solar, SoloPower Systems, and MiaSolé. Flexible Cadmium Telluride (CdTe) and Copper Indium Gallium Selenide (CIGS) thin film cells have achieved sunlight-to-DC electric power conversion efficiencies of more than 21% at the cell level, and can provide 16% efficiency at the array level to generate desired power densities of up to 216 W/m^2 at 1 A.U. from the sun. Thin film amorphous silicon cells, by contrast, have efficiencies below 10% at the array level.

CIGS technology was chosen for the current Brane Craft design due to the thinner stack height of a CIGS cell (~5 microns) compared to a CdTe cell (8-10 microns). An additional advantage of CIGS solar cell technology is that CIGS cells have the required total integrated dose (TID) radiation tolerance needed for this mission; they have been shown to tolerate a TID of 100 kilograys (10 megarads).[6]

Power conditioning and peak power tracking will be done using thousands of individual cells connected in various serial/parallel combinations to match the instantaneous output voltage requirements under current lighting conditions. The direct drive approach requires that ~36 cells be connected in series for

generating 20 V, and ~2200 cells be connected in series to generate 1,200 V. This approach eliminates the need for inductors and large capacitors, but it does require thin film transistors and associated logic to perform power switching. Fortunately, thousands of cells, plus diodes, transistors, and connecting "wires" can be fabricated in parallel on a single substrate. Thin film bypass and blocking diodes are required to handle shaded or open cells. These diodes are also needed to provide tolerance to the dozens of micrometeroid impacts that will occur during each mission.

Thin Film Electronics

Thin film transistors (TFTs) are a key enabler of Brane Craft electronics. TFT arrays were developed primarily for flat panel display applications with size ranging from about 1 cm (eyepiece displays used in digital cameras) to over 3 meters (110" televisions). Fabrication of mass-market displays occurs primarily in South Korea, China, Taiwan, and Japan. Current fabrication plants create multiple displays (6 to greater than 30) on pieces on glass with an area of about 9 square meters. Next generation (Gen 11) fabrication centers, or foundries, will cost about $7 billion USD and are expected to process 90,000 multi-display panels per month.[7] Fortunately, this level of investment is not required for 1 square meter and smaller Brane Craft; we will need to pattern significantly smaller substrates.

A modern 4K UHD television or monitor has at least 3,840 x 2,160 pixels, three color subpixels per pixel, and at least one TFT per pixel to control them; 24.9 million transistors deposited on a glass surface. These TFTs are fairly slow compared to conventional silicon nanoelectronics; the required switching speed for a 120 Hz UHD display is only 400 kHz while transistors manufactured on single crystal silicon substrates can easily exceed 4 GHz. Brane Craft need a minimum transistor switching speed of about 10 MHz, and preferably, 50 MHz. This is based on the micro-controller speeds we use in our AeroCube CubeSats for command and control, attitude determination and control, and communications.

The TFTS in current generation flat panel displays are an order-of-magnitude too slow (~400 kHz vs. ~10 MHz). They are typically fabricated using hydrogenated amorphous silicon (a-Si:H), and have gate lengths of about 30 microns. Speed can be significantly increased by changing the semiconductor material and by shrinking transistor size. The maximum switching frequency f_{max} of a thin film transistor is given by:

$$f_{max} = \mu * V / L^2 \qquad (1)$$

where μ is the carrier mobility, V is the switching voltage, and L is the gate length; the distance between the source and drain gates of a field-effect transistor. Carrier mobility of a-Si:H in flat panel displays is about 0.6 cm^2 / V-s; about 300 times worse than the hole mobility in single crystal silicon.

Due to the maximum 10 megarad TID expected for almost unprotected thin film electronics over one month in low Earth orbit, I originally chose ZnO as the semiconductor. Sputtered thin film ZnO layers have shown carrier mobilities in excess of 50 cm^2 / V-s.[8] Thin film carbon nanotube transistors (CNTs) can also provide tens of megarad total dose tolerance with high mobility. Researchers at Lockheed Martin Space Systems Company, and The Aerospace Corporation, demonstrated CNT transistor operation to 21 megarads.[9] Inkjet-printed CNT transistors on flexible substrates have demonstrated carrier mobilities up to 9.8 cm^2 / V-s.[10] Both CNT *and* ZnO transistors will be required to create p-type and n-type transistors for conventional CMOS circuits. Figure 7 shows calculated cutoff frequencies as a function of gate length for a-Si:H with a 0.6 cm^2 / V-s mobility and the proposed ZnO or CNT transistors with a degraded mobility of 5 cm^2 / V-s.

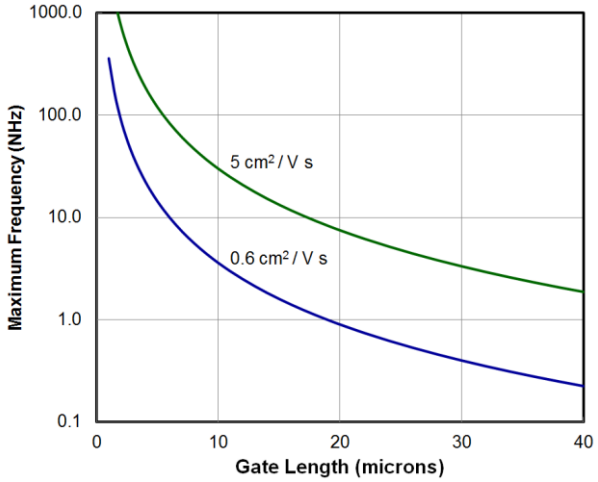

Figure 7. Maximum speed of thin film transistors as a function of gate length for hydrogenated amorphous silicon (lower curve), and ZnO or CNT semiconductors (upper curve) and a 6 V cutoff voltage.

Figure 7 shows that ZnO and inkjet-printed CNT transistors can operate at frequencies in excess of 30 MHz with a gate length of 10 microns or less. Features of this size (10 microns) can be lithographically patterned using relatively inexpensive photomasks, or direct-printed using high-resolution inkjet technology. They can be fabricated on flexible substrates, or

fabricated on a rigid substrate with a flexible layer as the top most layer, and a sacrificial layer between the electronics and rigid substrate that gets dissolved at the last step. ZnO TFTs have been fabricated on 5-micron thick polyimide using this process.[11]

About 75 cm^2 of surface area is required for a nominal 500,000 transistor, 8 million instruction per second, thin film processor fabricated using a 10-micron process. This seems large, but over 130 could be deposited on one side of a 1 sqaure meter Brane Craft. Six processors could be deposited on each side using only 5% of the total 1 m^2 surface area. Processor dimensions could be cut in half, and required surface area reduced by a factor-of-four, by using to a 5-micron process.

Fabrication of conventional transistors and TFTs is typically done using a subtractive process:

- an individual layer of a dielectric, conductor, or semiconductor is deposited on a substrate using vacuum or liquid deposition,
- the deposited layer is covered by a thin layer of photoresist,
- the photoresist is hardened by heating in a vacuum,
- the entire substrate is exposed to ultraviolet light through a photomask,
- the photoresist is exposed to a liquid developer that removes photoresist over the unwanted regions,
- the exposed regions are removed using selective plasma or liquid etching,
- the remaining photoresist is dissolved and removed, and
- the surface is cleaned for the next layer.

Note that there are eight steps for every layer, and these steps may require liquid or vacuum processing. The advantage of this approach is that it doesn't care how many devices are fabricated on a substrate, as long as the photolithographic resolution and layer thicknesses are suitable for creating functioning devices; fabrication speed is independent of design complexity for a given number of layers. The disadvantages of this approach are that photomasks must be generated, multiple processing stations, e.g., thermal evaporators, sputtering chambers, photo exposure chambers, etc., are required, and the substrate must be transferred to all of these stations in a clean environment. Photomasks come in a variety of sizes, and inexpensive 5-micron resolution photomasks are readily available at sizes up to 10" square.

Additive manufacturing of electronics is relatively new. In this case, an industrial inkjet printer deposits a patterned 2-dimensional layer of conductor, semiconductor, or dielectric on a rigid or flexible substrate in aqueous form that dries into a solid structure.[12] This approach has been used to fabricate CNT transistor circuits using a solution of semiconducting single wall CNTs. These solutions are typically >98% semiconducting, and are fairly expensive at ~$500/milligram in solution due to the extra processing steps required to remove the 33% of metallic CNTs that result from typical arc-discharge CNT fabrication. Another additive process is screen printing. This has been used to make flexible, active-matrix electrochromic displays with CNT TFTs.[13]

These should be the least inexpensive methods for manufacturing radiation-hard, thin film electronics for Brane Craft in thousand-unit quantities. The majority of industrial inkjet systems have resolutions of less than 1600 dots per inch, resulting in minimum feature sizes of 16 microns and larger. This is borderline for printing 10-MHz processors. However, at least one system has been identified that can produce 5-micon minimum features, on a 30 cm x 30cm substrate.[14] In any case, limiting substrate dimensions to 12 inches or smaller will significantly reduce development and production costs.

Electrospray Thrusters

NASA's Space Technology Mission Directorate (STMD) funded development of micro-electrospray thrusters at MIT, NASA-JPL, and Busek Co., Inc. under the Game Changing Development Program.[15] Electrospray thrusters use applied electric fields on the order of 1 V/nm to electrodynamically pull a conducting liquid into a "Taylor Cone" with a ~3-nm radius sharp tip at the apex. This sharp tip further amplifies the applied electric field by about an order-of-magnitude, thus generating ~10 V/nm fields that directly field ionize the liquid molecules. This ionization process is extremely efficient and can yield ion currents of 500 nA or more per tip. Thrust is between 6 and 20 nanonewtons per tip for specific impulse (I_{sp}) between 2000 and 5000 s. Overall thrust scales as the number of active tips.

It's important to realize that ion current per tip, which is proportional to thrust, is independent of overall Taylor cone size. It should therefore be possible to create nano-electrospray thrusters with smaller Taylor cones and significantly reduced overall dimensions. Recent molecular dynamics simulations of electrospray thrusters performed at Penn State showed Taylor cone formation with 500 nA ion currents using base diameters as small as 12 nm with tip base-to-extractor

distances of less than 0.07 microns.[16] These simulations used the ionic liquid EMIM-BF_4 flowing out of platinum capillaries. Nano-electrospray thruster arrays can be thin film structures a few microns thick, and a few millimeters or less in lateral dimension. With a thrust of about 13 nanonewtons per tip at 4000-s I_{sp}, an 8 mm x 8 mm array with 10-micron lateral spacing between tips could generate 8.2 millinewtons of thrust using 630 thousand emitters. Input power is 180 W.

Micro-electrospray thrusters are still under development, and their current operating lifetime is between 10 and 100 hours. More development is needed, but this is already being funded by NASA. For this study, I focused on the propellant storage issues. The dielectric strength of 25-micron thick Kapton® is 303 kV/mm, yielding an estimated breakdown voltage of 2.1 kV and 3.8 kV for 7-micron and 12.5-micron thick Kapton® sheets, respectively.[17] Using the thicker Kapton® for the main structural sheets would give improved breakdown voltage margin, and further reduce the number of particle penetrations into the propellant chamber. Effective Kapton® thickness increases to 49 microns, and wet mass increases to 96 grams.

Particle penetration into the propellant storage layer is not a problem for propellant storage since the vapor pressure of the ionic liquid propellants is essentially zero, and capillary action should hold the propellant in for 10-micron scale holes. The more serious concern is shorting a grounded spacecraft outer layer with a propellant that can be at +1,200 or -1,200 Volts; propellant potentials when a thruster is operating. Ionic liquids are conductive, and the storage areas should be electrically isolated from the immediate propellant next to a thruster. The spacers in Figure 6 provide this electrical isolation. A Brane Craft still needs a way to transfer propellant between storage regions and thruster regions. Providing propellant transfer capability and kilovolt electrical standoff is an issue that still needs to be addressed. Potential solutions include isolation valves based on localized freezing, since a solid ionic liquid is non-conducting and the isolation is only needed while thrusting, and bubble-based droplet ejectors used in some inkjet printers.

Sensors

A number of simple sensors can be fabricated as thin film structures. The first is the strain sensor. This device is composed of a thin conductive trace that meanders back and forth to fit a much longer length onto a shorter footprint. Trace length along one direction should be much longer than the trace length perpendicular to that direction. If the substrate is stretched along the long direction, the resistance will change. Figure 8 shows the basic layout and Wheatstone bridge readout circuit used to monitor strain in the horizontal direction. All resistances should be equal in the unstrained state, and the potential difference, or $V_{measured}$ would be zero. If the substrate is strained, $V_{measured}$ will be positive or negative, and proportional to the strain. Typically, three sensors with their long axes tilted by 60° to each other are used to determine orthogonal X and Y strains in the plane of the sensor. Commercial strain sensors are small Kapton® or plastic sheets with an adhesive layer on one side so that they can be physically bonded to the structure to be monitored. In our case, the Kapton® is the structure to be monitored. Twenty or more sensors deposited on the structural sheets can be used to monitor local strain and determine local and overall spacecraft curvature. Due to their simplicity and lack of semiconductors or critical dielectrics, these sensors should be very radiation-hard. The electronics to process the voltages will, however, need to be radiation hard to many megarads.

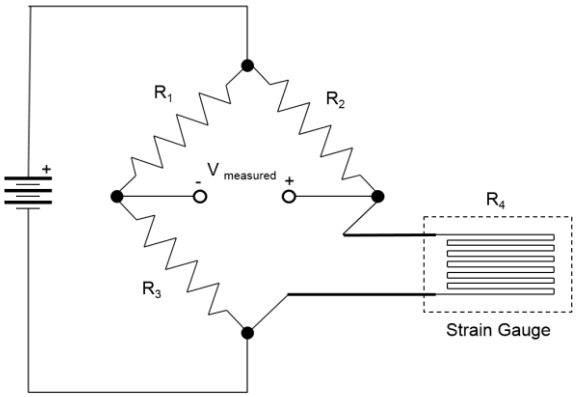

Figure 8. Circuit diagram of a single-axis strain sensor and Wheatstone bride readout circuit.

Another useful, simple sensor is a giant magnetoresistive sensor for measuring magnetic field magnitude in a particular direction. We fly commercial versions, which typically include three orthogonal axes, amplifiers, and digital output in an integrated circuit, in our CubeSats in LEO. These sensors use two ~10-nm thin layers of ferromagnetic material separated by a ~5-nm thick non-magnetic conducting layer like copper or aluminum.[18] This sandwich is usually deposited as a narrow rectangle as seen from above the substrate. The resistance across the long axis of the stack can be altered by changing whether the moments of the ferromagnetic layers are parallel or antiparallel; antiparallel layers increase resistance. A low current (~a few mA per micron of width), flowing along the long dimension puts the magnetic domains in the ferromagnetic layers in an antiparallel configuration.

An external magnetic field can make them parallel, thus changing the resistance. These sensors typically have a range of 0.001 to 10 Oersteds that is well suited to measuring the Earth's magnetic field in LEO. Again, due to their simplicity and lack of semiconductors or critical dielectrics, these sensors should be very radiation-hard.

An important attitude sensor is a sun sensor shown schematically in Figure 9. For this application, ~10 microns of Kapton® will separate the aperture plate from the quad detector. Thin Kapton® sheets look orange, and are at least 80% transmissive across the 700 nm to 1,100 nm wavelength range. Typical quad cell detectors are single crystal silicon photodiodes, but we'll need a carbon nanotube or CIGS equivalent for the high radiation environment. One group has achieved 1% conversion of sunlight into DC power using C_{60} Buckyballs on 5-nm thick single wall carbon nanotube layers, with 45% external quantum efficiency between 1,000 and 1,100 nm wavelengths.[19] This can work in our application, but no radiation tolerance data exists.

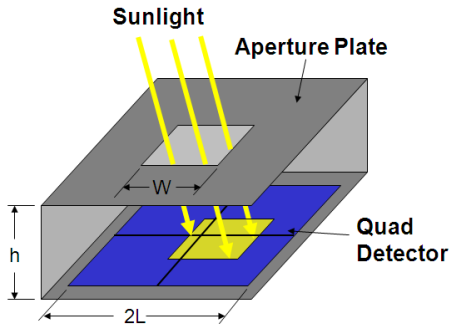

Figure 9. Schematic diagram of a sun sensor.

Earth sensors are another useful attitude determination sensor. They typically use thermal infrared detectors; the Earth is a warm ball at roughly 300 K while space is at 3 K. Microbolometers have become the detector of choice since they don't have to be cooled, and can be made in arrays for thermal imaging. Typical devices use a window or focusing lens to transmit thermal radiation between 5 and 14 microns in wavelength. Kapton® absorbs at those wavelengths, so an open hole would be the best geometry. Multiple detectors distributed across the surface, combined with surface warping, could locate the direction of the center of the Earth. Microbolometer detectors using single wall carbon nanotube networks have shown responsivities of up to 250 V/W.[20] Typical thermal radiation fluxes in LEO are about 200 W/m^2, so the thermal radiation getting through a 40-micron diameter hole in a 10-micron thick layer of Kapton® is 0.25 mW, and the output response would be ~60 μV. This can be amplified to Volt output levels.

Shape Control

Brane Craft have to wrap around a debris object, but they also need curvature to maintain some degree of structural rigidity. Curvature applied along one edge of the Brane Craft can mechanically stabilize it against bending moments due to thrusting. This is similar to holding a sheet of paper between thumb and index plus middle fingers, thus forcing local curvature, when extending the sheet horizontally to another person.

Curvature can also be applied throughout the square-meter structure to make an effectively rigid spacecraft.

Sheet curvature is also essential to collect sunlight while thrusting in any direction. Electrically-propelled spacecraft use gimbals on solar arrays and sometimes on thrusters to maximize power collection while thrusting. Brane Craft don't have gimbals, by they can warp their geometry to accomplish the same thing. Figure 10 shows the Brane Craft configuration when thrusting and not holding a debris object; the outbound configuration while thrusting. In this case, it is thrusting normal to the incident solar radiation. The whole spacecraft can rotate about the spacecraft-sun line, so this configuration can thrust in any direction that is perpendicular to the incident solar radiation. Figure 11 shows options for thrusting towards, against, and at right angles to incident solar radiation. Since Brane Craft can rotate about a vertical axis in this figure while maintaining the same solar collection, thrusting in any direction while maintaining 80% or more solar collection is possible.

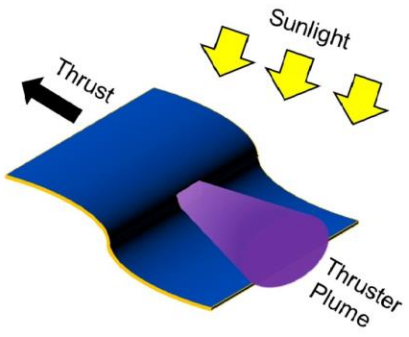

Figure 10. Schematic drawing of a Brane Craft thrusting normal to the direction of sunlight.

Brane Craft must also be able to thrust while curled around a debris object. In this case, the Brane Craft becomes a tube as shown in Figure 12. The axis of symmetry is perpendicular to the incoming solar radiation to maximize power. In this case, maximum

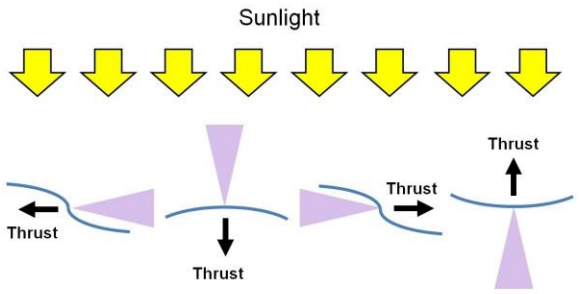

Figure 11. Four Brane Craft shapes and orientations to maximize solar collection while thrusting in four different perpendicular directions. Sunlight comes straight down from the top and each Brane Craft extends 1 meter into the page; there is no curvature in this direction.

power generation is $(1/\pi) * 200\ W = 64\ W$. The Brane Craft can rotate about the sunlight vector, and about the axis of symmetry. Since these are two orthogonal axes, the primary thruster array can generate thrust in any direction.

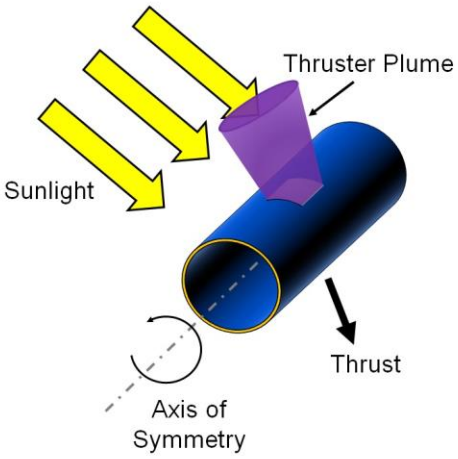

Figure 12. Rendering of a Brane Craft curled about a debris object (not seen in this image) while thrusting.

ACTIVE ORBITAL DEBRIS REMOVAL

Brane Craft will most likely be launched as secondary payloads due to their inherently low mass. The International Space Station (ISS) makes a good starting point for the deployment of Brane Craft due to the significant number of ISS resupply missions launched each year. I therefore used a nominal starting orbit of 400 km circular with a 51.6° inclination for mission analyses.

Waiting for RAAN Alignment

Once a target debris object is identified for a particular Brane Craft, it must wait until the orbital mechanics for rendezvous are favorable. Rendezvous requires matching of the Brane Craft three-component velocity vector and three-component position vector to the target object at a certain time; basically matching all six orbit elements at the correct time. Semi-major axis, eccentricity, and inclination are directly changed by active thrusting. The Right Ascension of the Ascending Node (RAAN) is the direction of the vector from the center of the Earth to the point where the northern-heading part of the orbit crosses a projection of the Earth's equator. For a given orbit inclination, it determines the plane of an inclined orbit in inertial space, and has a range of 0° to 360°. While a spacecraft can change RAAN through direct thrusting, it can be extremely propellant expensive. To change RAAN by 180° at 400-km altitude, for example, requires a delta-V of twice the orbital velocity: 2 x 7.67 km/s = 15.4 km/s. This would exhaust almost all of the Brane Craft propellant. Fortunately, orbital mechanics provides a more propellant-efficient solution.

Orbit planes rotate about the Earth's spin axis at a rate determined by orbit altitude, inclination, and orbit eccentricity. Figure 13 shows the westerly RAAN rotation rate, or nodal regression rate, in degrees per day as a function of altitude for circular orbits for multiple orbit inclinations. Orbits with inclinations between 0° and 90° rotate westward while those at inclinations greater than 90° rotate eastward. Sun-synchronous orbits rotate eastward at a rate of 360°/365.24 days = 0.9856° /day, irrespective of orbit altitude. Data points for the ISS and 700-km sun-synchronous orbits are shown, and the difference in nodal regression rate between these two orbits is 6.00°/day. A Brane Craft at the ISS would have to wait between 0 and 60 days before starting an up leg trajectory in order to properly match the RAAN of a debris orbit in a sun-synchronous orbit of any altitude. Target objects at lower orbit inclinations could require a year or more of waiting. Fortunately, ISS orbit is a fairly benign place to wait.

The Outbound Leg

The outbound leg will require a change in altitude and inclination, while the inbound leg requires only a change in altitude, or more specifically, semi-major axis. Figure 14 shows the delta-V requirements to go from a starting orbit at 400 km to a higher LEO orbit with orbit inclination changes of 0°, 10°, 20°, 30° and 40°. These are based on Hohmann transfer calculations with an optimized split of inclination changes between the lower and upper burns.

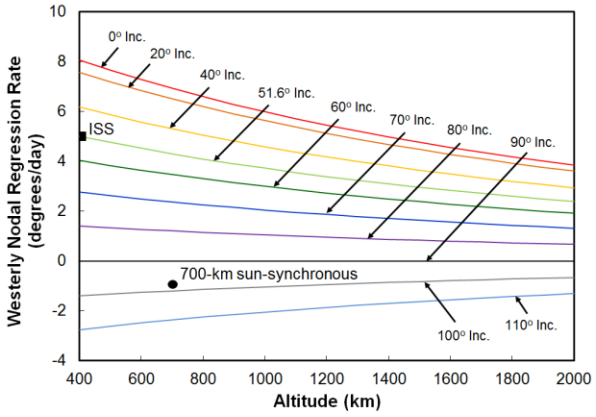

Figure 13. Westerly nodal regression rate in degrees per day as a function of altitude for circular orbit inclinations of 0°, 20°, 40°, 51.6°, 60°, 70°, 80°, 90°, 100°, and 110°.

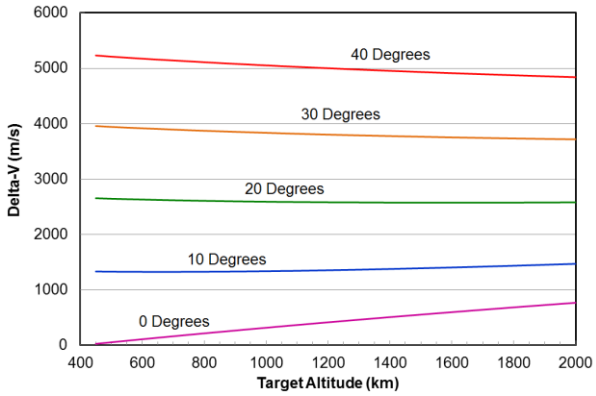

Figure 14. Delta-V required to go from a 400-km circular orbit to a higher circular orbit with inclination changes of 0°, 10°, 20°, 30°, and 40°.

Figure 14 shows that inclination changes dominate the outbound delta-V requirements in LEO when they are 10° or larger. For inclination changes between 10° and 30°, it makes little difference what the target altitude is, and for inclinations in excess of 20°, the delta-V actually drops with increasing altitude. For a fresh Brane Craft starting at 400-km altitude with a 16-km/s delta-V capability, about 15.5 km/s, 14.6 km/s, 13.4 km/s, 12.2 km/s, and 11.0 km/s are available for the deorbit phase, or inbound trajectory, for a target altitude of 1000 km and target inclination changes of 0°, 10°, 20°, 30° and 40°, respectively. By comparison, the remaining delta-V capability for a fresh Brane Craft starting at ISS orbit (400-km altitude, 51.6° inclination) and going to geostationary orbit (35,786-km altitude, 0° inclination) is 11.2 km/s.

Figure 14 shows that the outbound trajectory can consume up to 5.2 km/s of delta-V for a 40° change in inclination. The Brane Craft will be in a curved, open configuration with an effective solar collection area normal to the incoming light, of 0.75 square meters. This provides maximum sunlight collection while still being able to point the thrusters along the flight direction (see section 4.1). Average power generation will be 150 W, with 130 W available for thrusting. Maximum thrust will be 5.9 mN during sunlit parts of the orbit.

Typical eclipse fraction in low Earth orbit is ~40%, but can reach 0% for a small fraction of orbits, especially at the high altitude end of LEO. Prograde thrusting, or thrusting along the velocity vector, adds energy to the orbit and normally results in a continuous increase in altitude along a spiral trajectory. Prograde thrusting while only in sunlight, however, will result in larger and larger elliptical orbits with increasing orbit eccentricity. Significant eccentricity growth will occur, and cannot be easily corrected until the orbit RAAN or argument of the perigee changes by 180°. This can take months. To minimize growth of orbit eccentricity, prograde thrusting should occur over equal orbit arcs that are approximately 180° apart in the orbit plane. Figure 15 shows that the best arc end locations are near the points where the spacecraft either leaves or enters sunlight. Each thrusting period occurs over α^o of the orbit, where α is a function of orbit altitude and inclination for circular orbits. Figure 15 shows the worst-case (smallest α) geometry where the orbit plane is edge-on to sunlight, and Figure 16 shows the orbit fraction over which thrusting can occur for this worst-case condition. For a 400-km circular orbit, α = 39.6° and outbound thrusting occurs over only 22% of the orbit.

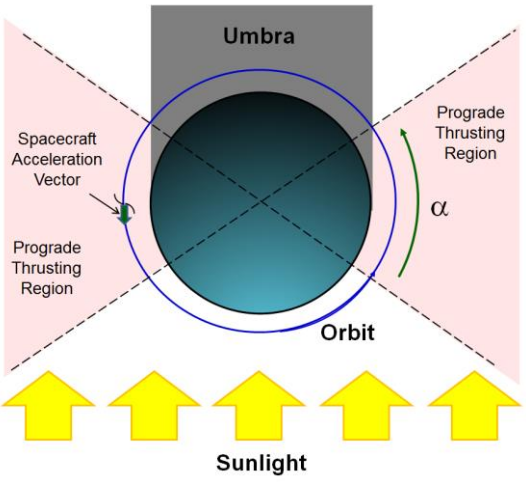

Figure 15. Schematic diagram of the eclipse geometry in LEO and optimum thrusting regions to provide balanced orbit raising using electric thrusters that only operate in sunlight.

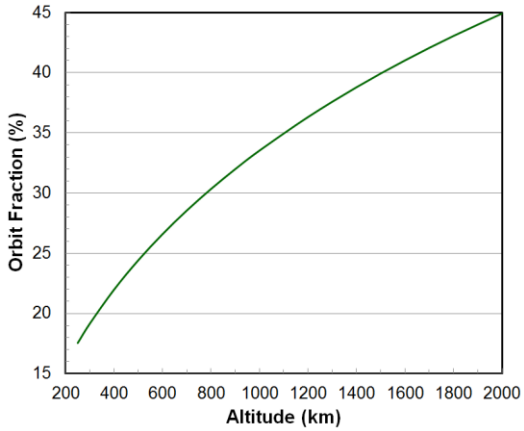

Figure 16. Orbit fraction during which prograde thrusting for symmetric orbit-raising can occur, under worst-case orbit orientation.

The major propulsion challenge during the outbound transfer, as shown in Fig. 14, is to change orbit inclination. This maneuver is most efficiently done within ~30° of where the orbit crosses the Earth's equatorial plane. Figure 17 shows a schematic drawing of the orbit geometry as viewed from the sun. The line of apsides connects these points, and one side of the line starting at the center of the Earth is the RAAN vector, and the other half is the anti-RAAN vector. The orbit and equatorial plane cross at two points separated by 180°, so there are two regions of favorable thrusting. The RAAN and anti-RAAN vectors are not usually parallel or anti-parallel to the sun-earth vector, so part of one is typically in shadow. This is illustrated in Fig. 17. At least one region will be in full sunlight, so a minimum orbit fraction of 60° / 360° = 16.7% can be used for inclination-change maneuvers. Note that inclination change thrusting is directed mostly perpendicular to the orbit plane as shown in the figure.

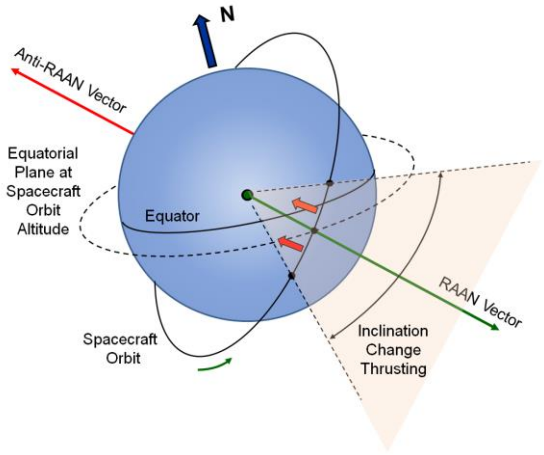

Figure 17. Orbit geometry for inclination change thrusting, as seen from the sun.

The longest orbit transfer times will occur for high delta-V transfers that are dominated by inclination change. In this case, the orbit average thrust is 16.7% of the 5.9 mN maximum thrust in the outbound configuration. Figure 18 shows calculated maximum orbit transfer time as a function of outbound delta-V up to 6500 m/s under these constraints. The longest outbound trajectory of 5 days at 6500 m/s is more than adequate to go from the ISS to any sun-synchronous orbit up to 2000 km in altitude.

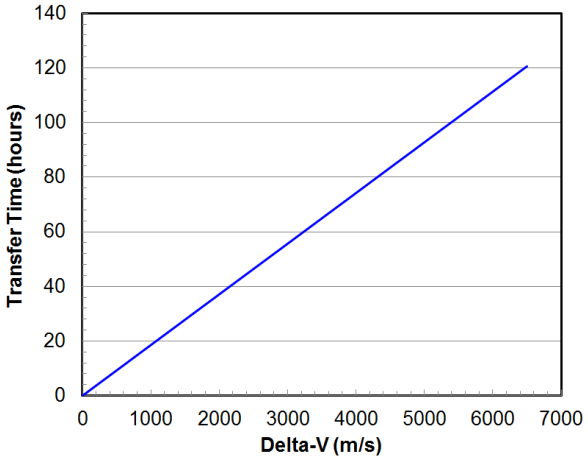

Figure 18. Maximum transfer time to reach debris object orbit as a function of outbound transfer Δ-V.

Rendezvous and Wrapping

Rendezvous is an orbit matching maneuver. This requires simultaneous matching of six orbital elements at a fixed time. Semi-major axis, eccentricity, inclination, RAAN, and argument of the periapsis will have been matched during the outbound thrusting maneuver. The Brane Craft and target object will be in the same orbit, but at different locations along that orbit at any given time. Position along an orbit is determined by the true anomaly. True anomaly of an individual satellite in circular orbit can be changed by temporarily moving to a different altitude, remaining at that altitude until the appropriate phase change has accumulated due to the different orbital period, followed by a return to the original altitude. The orbital period τ is given by:

$$\tau = 2\pi\,(a^3/\mu_E)^{1/2} \qquad (2)$$

where a is the semi-major axis and μ_E is the gravitational constant G times the mass of the Earth M_E which is numerically equal to 398600.44 km^2/s^2. The phase (true anomaly) change $\Delta\nu_d$ that occurs while occupying a different altitude drift orbit is given by:

$$\Delta\nu_d = 2\pi\, t_d\,(\tau_0 - \tau_1)/\tau_0\,\tau_1 \qquad (3)$$

where t_d is the time at new altitude, τ_0 is the original orbit period and τ_1 is the orbit period at the new altitude. Increasing altitude results in an *increased* orbit period and a *decreased rate of change* in true anomaly, compared to the target orbit.

Maneuver velocity increment as a function of maneuver time was calculated using the approach outlined above and detailed in Reference 21. Figure 16 shows velocity increment as a function of maneuver time for an 180° phase change in a circular orbit at 600, 1000, and 2000-km altitude. This is the largest possible phase change. A Brane Craft can perform this maneuver in a day, but the delta-V is significant at about 500 m/s. Practical rephasing times are 3 to 8 days.

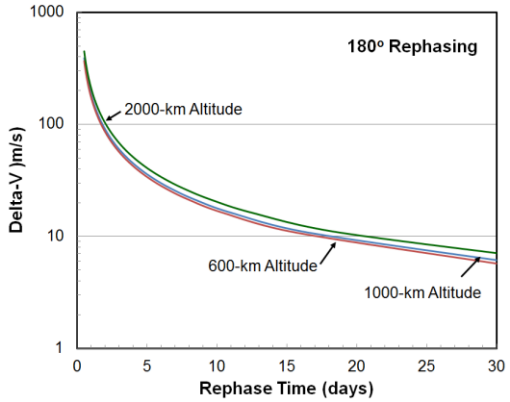

Figure 19. Delta-V required to change true anomaly by 180° as a function of time for 600 km, 1000 km, and 2000 km circular orbits.

The final step is to maneuver close enough to the target object to wrap around it. Physical wrapping takes seconds, but the maneuvering part can take a couple days. Overall, the outbound leg, with rendezvous and final wrap around, will require up to fifteen days.

The Inbound leg

At this point, the Brane Craft has cylindrically wrapped itself about the target object, and thrusts in the anti-flight direction while in sunlight. The inbound leg does not require any inclination changes, and the thrusters can operate continuously since any eccentricity changes will reduce deorbit time. Remaining delta-V capability, based on the initial 81-gram wet mass, is 9 to 16 km/s.

Since the combined mass of the Brane Craft plus target object is larger than the initial 81 gram wet mass, and thrust levels are lower due to the change in geometry, the inbound trajectory can take longer than the outbound trajectory. Figure 20 shows calculated inbound orbit transfer time as a function of remaining delta-V based on the initial wet mass, for a Brane Craft carrying the maximum debris object mass.

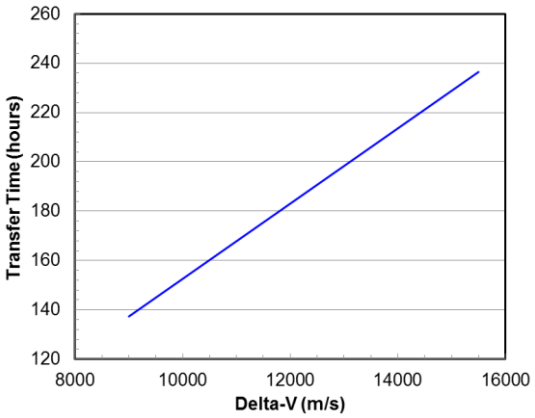

Figure 20. Inbound transfer time to a 250-km disposal orbit for a Brane Craft carrying the maximum debris object mass as a function of remaining delta-V at the beginning of the inbound transfer.

Maximum debris object mass as a function of circular debris orbit altitude for remaining delta-Vs of 11, 13, and 15 km/s are given in Figure 21. These calculations were based on a 250-km circular disposal orbit and thrusting continuously while in sunlight. From an ISS starting orbit, all debris objects in LEO up to 1 kg in mass could be deorbited using the current Brane Craft design if the debris inclination is within 38° of the ISS inclination; 13.6° to 89.6°. For sun-synchronous in LEO, this drops slightly to 0.9 kg. All debris objects up to 2 kg in mass could be removed from altitudes up to 1000-km. Maximum inbound transit time is 10 days.

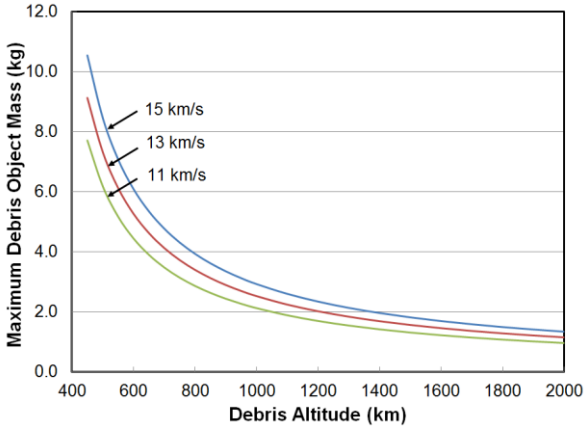

Figure 21. Maximum debris orbit mass that can be taken down to 250-km altitude as a function of initial debris altitude for remaining Brane Craft delta-V reserves of 15, 13, and 11 km/s using the current Brane Craft design.

Figure 22 shows apogee and perigee profiles of an inbound orbit transfer simulation run using The Aerospace Corporation's Satellite Orbital Analysis Program (SOAP). This simulation started at a 900-km altitude, 99.0° inclination, circular, sun-synchronous orbit and fired thrusters at a 2.0 mN thrust level at 4000s specific impulse, anti-parallel to the flight direction, while the spacecraft was in sunlight. Initial mass at 900-km altitude was 2.27 kg; 70-grams for the Brane Craft after reaching the debris orbit, plus 2.2 kg of debris object mass. The Brane Craft consumed 6 km/s of delta-V getting there from the ISS orbit, leaving 10 km/s for the inbound leg. Atmospheric drag was included, with an average cross section of 0.1 m^2; minimum area for a curled up Brane Craft carrying a debris object is 0.07 m^2. Re-entry occurred 143.9 hours after the start of the deorbit maneuver, with less than 1% propellant remaining. The estimate from Fig. 20, which did not include eccentricity buildup, was 152.6 hours; only 6% longer. The perigee drops linearly from 900 km to 130 km, while the apogee drops at a slower rate, until the perigee reaches 200-km altitude where atmospheric drag brings down the apogee more rapidly.

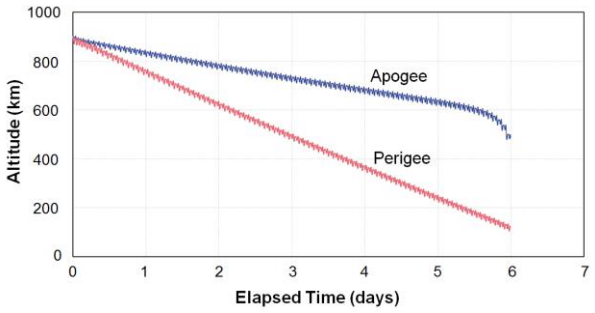

Figure 22. Apogee and perigee evolution during an inbound transfer of a 2.2-kg mass debris object in an initial 900-km, sun-synchronous, circular orbit.

Another SOAP deorbit simulation was performed for a 2.13 kg mass Brane Craft with debris object in a 1,400-km altitude, 52° inclination, circular orbit. In this case, the delta-V required to reach this orbit from the ISS is only 550 m/s, leaving a delta-V reserve of 15,450 m/s. The maximum mass debris object is 2.13 kg for this orbit. Figure 23 shows the evolution of apogee and perigee over time. Re-entry occurred 212.8 hours after the start of the deorbit maneuver, with less than 1% propellant remaining. The estimate from Fig. 17 was 235.7 hours; 11% longer. The perigee drops linearly from 1400 km to 110 km, while the apogee once again drops at a slower rate, until the perigee reaches 200-km altitude where atmospheric drag brings down the apogee more rapidly.

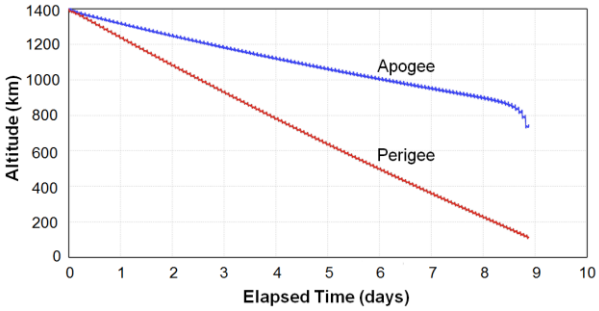

Figure 23. Apogee and perigee evolution during an inbound transfer of a 2.13-kg mass debris object in an initial 1,400-km, 52° inclination, circular orbit.

ENVIRONMENTAL CONCERNS

Radiation

The LEO environment, and outer space in general, is filled with energetic subatomic particles that can degrade and disrupt the proper operation of electronics and living organisms. The major particle populations are electrons and protons trapped by the Earth's magnetic field, and Galactic Cosmic Rays (GCRs) consisting of relativistic protons and heavier atomic nuclei. These high-energy particles deposit energy in the host material, leading to ionization and dislocation of host nuclei. Energy deposition is expressed in rads, where a rad is the ionizing particle dose that deposits 100 ergs of energy per gram of target matter, typically silicon. The SI unit is the gray, where 1 gray = 100 rads.

Electronics are degraded by particle radiation, and this damage accumulates over time. The time integral of the energy deposition is called the Total Ionizing Dose (TID), and the maximum TID that a particular type of electronics can withstand is a function of device materials and construction. Typical values are 1 to 10 kilorads for commercial electronics. Figure 24 shows the dose rate in rads/year in silicon, as a function of aluminum shielding thickness, in a 700-km sun-synchronous (98.19° inclination) circular orbit due to trapped particles. Data for this plot was generated by the SPace ENVironment Information System (SPENVIS) supported by the European Space Agency (ESA).[22] Trapped proton and electron fluxes and energy distributions were calculated using the AP-8 trapped proton and the AE-8 trapped electron models for January 1, 2020 through December 31, 2020. Total ionizing dose was calculated in silicon using the SHIELDOSE-2 model for a semi-infinite geometry.

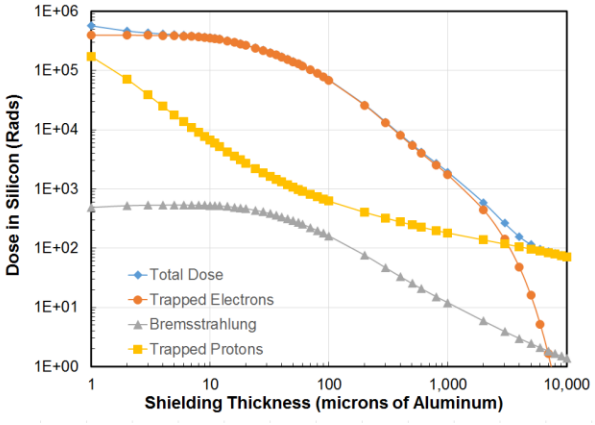

Figure 24. Yearly dose rate in rads/year in silicon as a function of aluminum shielding thickness for a 700-km circular, sun-synchronous (98.19º inclination) orbit.

The radiation dose has three components: electrons, protons, and "braking radiation" (bremsstrahlung); photons generated by the slowing down of protons and electrons. For this orbit, trapped electrons dominate the dose for shielding thicknesses less than 3 mm. Most spacecraft have from 1 to 5 mm (1,000 to 5,000 microns) of aluminum shielding, so electronics with a maximum 5 kilorad TID could function from 2.5 through 43 years in this orbit. Brane Craft have significantly less shielding; about 10 microns of Kapton® above the electronics and 30 microns below. In this orbit, based on the electron and proton energy spectra and the energy absorption characteristics of Kapton®, the equivalent aluminum thicknesses are 6 microns above and 18 microns below.

Figure 25 shows the calculated yearly dose in silicon for a Brane Craft as a function of altitude for 0º, 30º, 60º, and 90º inclination orbits. These dose rates were obtained by adding the semi-infinite slab dose rates for 6 microns and 18 microns of aluminum shielding, at each altitude and inclination. Figure 25 shows maximum yearly total dose values of 190,000 rads at 400-km altitude to 92 megarads at 2000-km altitude. The vast majority of orbital debris lie between 60º and 90º inclination, so the upper limit can be relaxed to 43 megarads per year. For a maximum of 3-weeks at this 2000-km altitude, the maximum total dose is 830,000 kilorads; well beyond the limit of conventional silicon electronics. Electronics with at least 1 Megarad TID tolerance is required, and preferably 10 Megarads for robustness and ability to linger at higher altitudes for months. At ISS orbit, similar calculations yield a much lower yearly total dose of 180,000 rads. Standard COTS Brane Craft electronics with a 5 kilorad TID limit would operate for up to 10 days in an ISS orbit.

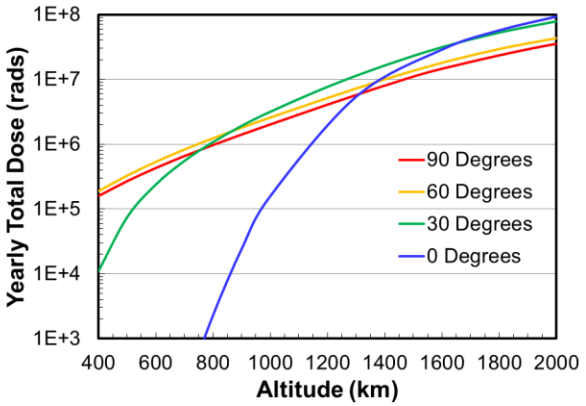

Figure 25. Yearly total dose rates as a function of altitude for 0º, 30º, 60º, and 90º inclinations for a Brane Craft with 10 microns of Kapton® shielding on one side, and 30 microns of Kapton® shielding on the other side.

Figure 26 shows yearly total dose results for a more conventional spacecraft, such as a CubeSat, with 1 mm of aluminum shielding. This is representative of some CubeSats with skeletal aluminum frames and circuit boards as shielding, and for sun and Earth sensor electronics behind a thin optical window. Overall, the dose rates are about 1000 times lower than for a Brane Craft. Conventional COTS electronics with a 5 kilorad TID limit would work for about a year at altitudes up to 1000 km. To go higher, thicker shielding is required.

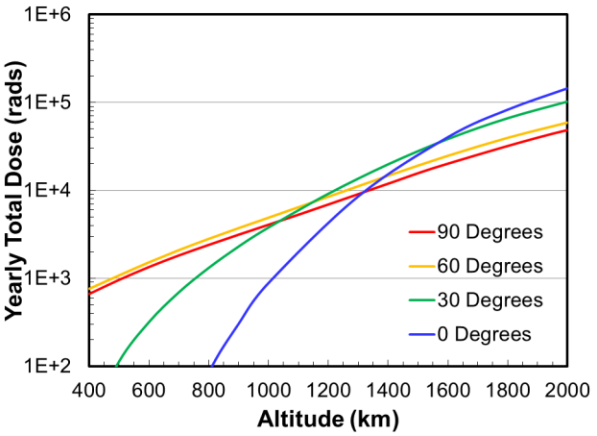

Figure 26. Yearly total dose rates as a function of altitude for 0º, 30º, 60º, and 90º inclinations for a conventional spacecraft with 1 mm of aluminum shielding.

Micrometeroid and Man-Made Impacts

The LEO environment is also full of micrometeoroids and micron-scale debris objects that can sever space tethers and perforate membrane spacecraft. Figure 27 shows the size distribution of micrometeoroids in a

1,200 km altitude circular orbit according to the Grün interplanetary flux and MASTER micrometeoroid and debris models available on SPENVIS.[23,24] The Micrometeoroid And Space debris Terrestrial Environment Reference (MASTER) model by ESA is the 2009 version that includes natural micrometeoroids plus man-made objects such as explosion fragments, collision fragments, paint flakes, solid rocket aluminum oxide particulates, etc., assuming "business as usual"; no anti-satellite tests or improved debris prevention measures. Note that the micrometeoroid flux for 10-micron diameter particles is 132 particles per year for a 1-square meter Brane Craft, 2 particles per year at 100-micron diameter, and 0.3/year at 200-micron diameter. Adding in man-made debris increases these numbers to 380/year for 10-micron diameter objects, 23/year for 100-micron diameter objects, and 2/year for 200-micron diameter objects.

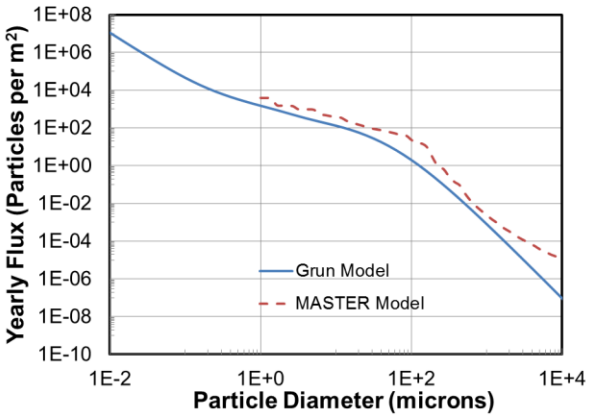

Figure 27. Yearly particle flux vs particle diameter in a 1,200-km altitude circular orbit according to the Grün and MASTER 2009 models.

What size particle can penetrate 10 and 20 microns of Kapton®? Gas gun experiments have shown that a hole diameter to thickness ratio of 2, indicative of penetration through a single wall or sheet, occurs at a particle diameter/thickness ratio of 0.7 for a 5 km/s soda-lime glass spherical particle impacting Kapton® at normal incidence.[25] At 5-km/s incident velocity, a 7-micron diameter particle would penetrate a 10 micron thick Kapton® sheet, and a 14 micron diameter particle would penetrate 20 microns of Kapton®. The critical mass m_c in grams, needed to penetrate a wall, for a particle with density ρ in g/cm^3 impacting at velocity V in km/s is given by:

$$m_c = [\, 2.54\, t / (K_t\ \rho^{1/6}\ V^{7/8})]^{1/0.352} \qquad (4)$$

where t is wall thickness in inches and K_t is a material constant, typically 5.4 for aluminum alloys.[26] Entering the velocity, thickness, density, and calculated mass based on particle diameter yields $K_t = 0.89$ for Kapton®. At V = 10 km/s, the critical particle diameters drop to 4 and 8 microns. Table 3 shows the critical diameters calculated using Eq. 4 to penetrate 10 and 20 microns of Kapton®, and the yearly rate of those penetrations, for impacting velocities of 5, 10, 14, and 20 km/s. The number of yearly impacts is lower at 20 km/s than the others because only micrometeoroids have these impact velocities. These numbers are for impacts normal to the surface of a one square meter sheet, and actual values will be lower; 50% lower is a good first estimate based on the average of the cosine over all impacting angles. Using this estimate, Table 3 shows that for a one-month long mission, a 10-micron thick Kapton® layer will be breached ~42 times. A 20-micron thick Kapton® layer will be breached ~21 times. The number of breaches can be reduced by a factor of 3 by leaving the Brane Craft curled up whenever possible.

Table 3. Critical particle diameters, and yearly impact rates per square meter for those diameters and larger, to penetrate 10 and 20-micron thick Kapton® sheets for normal incident velocities of 5, 10, 14, and 20 km/s.

V (km/s)	D_c for 10μ Kapton® (μ)	D_c for 20μ thick Kapton® (μ)	Pentrating Yearly Impacts for 10μ Kapton®	Penetrating Yearly Impacts for 20μ Kapton®
5	7	14	480	230
10	4.1	8.2	970	400
14	3.1	6.2	1000	500
20	2.4	4.8	600	270

Thermal Environment

Brane Craft are two-dimensional spacecraft with almost no thermal mass. They will cool down rapidly after entering eclipse, to settle at a temperature primarily determined by the absorptivity/emissivity properties of the solar cells. A simulation of overall Brane Craft temperature was run using a 1350 W solar flux, a 200 W thermal flux from the Earth, a Kapton® specific heat of 1.09 J-gram/K, an EMIM-BF4 (1-Ethyl-3-methylimidazolium tetrafluoroborate, the conventional ionic liquid propellant) specific heat of 1.9 J-gram/K, an absorptivity of 0.8, and an emissivity of 0.8. This simulation used the current Brane Craft structural mass

of 54 grams, plus a full load of 27 grams of propellant. The simulation, shown in Figure 28, starts with the Brane Craft normal vector pointing at the sun for maximum power and heating, and then turning towards the Earth as it enters eclipse at T =29 seconds, again for maximum heating. The equilibrium temperature is 342 K (+69° C) while in sunlight, and drops to 205 K (-67° C) while in eclipse. Most of the cool-down occurs over 2 minutes. The high temperature is acceptable, but the low temperature will freeze EMI-BF4 ionic liquid propellant. Its freezing point is 298 K; 15° C. This simulation did not include the heat of fusion of the propellant to show a representative cool-down time constant for a non-freezing propellant.

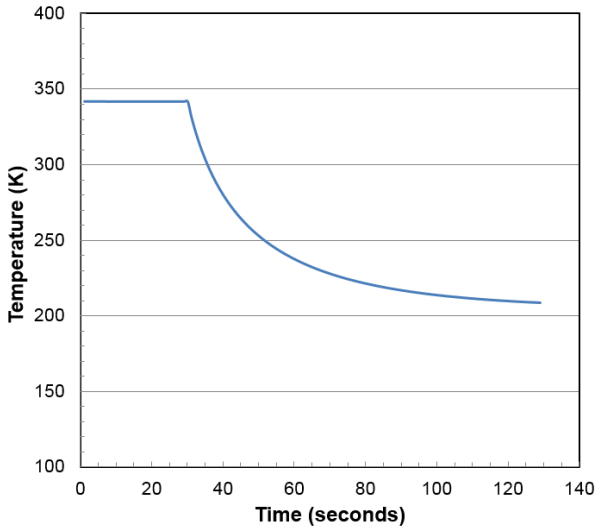

Figure 28. Temperature vs. time for a Brane Craft initially in full sunlight, and entering eclipse at T= 29 seconds.

Ionic liquid propellants were surveyed to find any that would not freeze at -67° C and have molecular weights (cation and anion) that were similar to the EMIM-BF4 values (molecular weight of 198), or lower. Heavier anions or cations would increase the required propellant voltage to achieve a 4000 s specific impulse, thus increasing the likelihood of dielectric breakdown. The ionic liquid 1-butyl-1-methylpyrrolidinium dicyan-amide is a potential candidate with a melting point of -90° C, and a molecular weight of 208. Another approach is to use eutectic mixtures of ionic liquids to induce freezing point depression.

SUMMARY

This work was funded by NASA's Innovative Advanced Concepts (NIAC) group during 2016. I performed initial mission analyses, which generated potential debris deorbit mission timelines and maximum masses that can be taken down from higher LEO orbits. I also evaluated environmental influences such as radiation, particle impacts, and thermal issues. Finally, I looked at various spacecraft systems to see if they were possible within the physical confines of a membrane spacecraft in a harsh environment.

This radical spacecraft design looks possible for active orbital debris removal, and potentially asteroid inspection and other future applications, but still has many remaining issues:

1. Can high-speed, flexible, thin-film electronics that can handle 10 megarad TID be manufactured at reasonable cost within the next decade?

2. Can sensor materials like photodiodes be made TID-tolerant to 10 megarad levels?

3. Can a "bullet-proof" spacecraft design be created where the bullets are high-speed micro-projectiles that generate ~50 through holes per month?

4. Can electroactive polymers or other "muscle" mechanisms provide required tensions and compressions to curl and control a Brane Craft?

5. Can communications systems be fabricated as thin-film systems? The basic electronics look possible, but some communications-system unique components such as crystal oscillators aren't amenable to thin-film design.

6. Can the overall design be scaled to arbitrary size (smaller and bigger)?

These will be evaluated through further analysis and experimentation during the 2-year long Phase II effort that was recently funded by NIAC.

Acknowledgments

I gratefully acknowledge the funding provided by NASA's NIAC program.

References

1. Thompson, Roger, "A Space Debris Primer," *Crosslink* (ISSN 1527-5264), The Aerospace Corporation, pp. 4-7, Fall 2015.

2. Hansen, B., Starchville, T., and Hoots, F., "First Responders in Space: The Debris Analysis Response Team," *Crosslink* (ISSN 1527-5264), The Aerospace Corporation, pp. 14-21, Fall 2015.

3. National Aeronautics and Space Administration, "Orbital Debris Quarterly News," **21**, #1, p. 12, February 2017.

4. Ailor, W., Chobotov, V., Peterson, G., and Patera, R., "Small Satellites: Space Debris and Reentry Hazards," Chapter 22 in **Small Satellites: Past, Present, and Future**, pp. 729-769, The Aerospace Press and the AIAA, Reston, Virginia, 2008.

5. Fraunhofer Institute for Solar Energy Systems, "Photovoltaics Report," Freiburg, Germany, November 2016, URL: https://www.ise.fraunhofer.de/de/downloads/pdf-files/aktuelles/photovoltaics-report-in-englischer-sprache.pdf

6. Pakkala, Asha Kiran, Pattabi, Manjunatha, Sanjeev, Ganesh, Fernandez, A.M., and Mathew, X., "A Study on the Radiation Resistance of CIGS/CdS Thin Film Solar Cell Against 8 MeV Electron," International Journal of Science Research, **1**, #4, pp.446-451, 2012.

7. TCL, "TCL Corporation to Toss $7 Billion to Build Gen 11 LCD and OLED Production Line in Shenzhen," Press Release #2016-09-02, TCL Corporation, Huizhou, China, September 2016, URL: http://www.tcl.eu/eu/newsroom/cl-corporation-to-toss-$7-billion-to-build-gen-11-lcd-and-oled-production-line

8. Brox-Nilsen, C., Jin, J., Luo, Y., Bao, P. and Song, A.M., 2013. Sputtered ZnO Thin-Film Transistors With Carrier Mobility Over 50. *IEEE Transactions on Electron Devices*, *60*(10), pp.3424-3429.

9. Ngo, Quoc X., Anderson, Scott A., O'Connor, Michael J., Nichols, Johnathan A., Dunning, James E., Holihan, Eric C., Taylor, Jerry C., Bushmaker, Adam, Walker, Don, and Mann, Colin J., "Scalable Carbon Nanotube Electronic Devices for Space Nanoelectronics Applications,"

10. Lee, D. *et al.,* "Logic circuits composed of flexible carbon nanotube thin-film transistor and ultra-thin polymer gate dielectric," *Sci. Rep.* **6**, May 2016.

11. Li, H. Y. U. and Jackson, T. N., "Oxide semiconductor thin film transistors on thin solution-cast flexible substrates," *IEEE Electron Device Letters*, vol. 36, pp. 35-37, Jan 2015.

12. Lee, D. *et al.,* "Logic circuits composed of flexible carbon nanotube thin-film transistor and ultra-thin polymer gate dielectric," *Sci. Rep.* **6**, May 2016.

13. Cao, Xuan, Lau, Christian, Liu, Yihang, Wu, Fanqi, Gui,Hui, Liu, Qingzhou, Ma, Yuqiang, Wan, Haochuan, Amer, Moh. R., and Zhou, Chongwu, "Fully Screen-Printed, Large-Area, and Flexible Active-Matrix Electrochromic Displays Using Carbon Nanotube Thin-Film Transistors," *ACS Nano* **2016** *10* (11), pp. 9816-9822, 2016.

14. Ceradrop Corporation, "X-Series CeraPrinter Data Sheet," Ceradrop Corporation, Limoges, France, 2016. URL: http://www.ceradrop.com/content/uploads/2016/04/2-X-SERIE_datasheet.pdf

15. NASA Space Technology Mission Directorate, "Micro-Electrospray Thrusters," 2013. URL: http://gcd.larc.nasa.gov/wp-content/uploads/2014/01/FS-MEP_factsheet_130124.pdf

16. Borner, Arnaud; Li, Zeng; and Levin, Deborah A., "Prediction of Fundamental Properties of Ionic Electrospray Thrusters Using Molecular Dynamics, *J. of Physical Chemistry*, **8**, #117, p.p. 6768-6781, 2013.

17. Dupont, "Summary of Properties for Kapton® Polyimide," Dupont, Inc., URL: http://www.dupont.com/content/dam/dupont/products-and-services/membranes-and-films/polyimde-films/documents/DEC-Kapton®-summary-of-properties.pdf

18. Caruso, Michael J., Bratland, Tamara, Smith, Dr. Carl H., and Schneider, Robert, "A New Perspective on Magnetic Field Sensing," Honeywell Inc, May, 1998, URL: https://aerocontent.honeywell.com/aero/common/documents/myaerospacecatalog-documents/Defense_Brochures-documents/Magnetic__Literature_Technical_Article-documents/A_New_Perspective_on_Magnetic_Field_Sensing.pdf

19. Shea, Matthew J., and Michael, Arnold S., "1% solar cells derived from Ultrathin Carbon Nanotube Photoabsorbing Films," Applied Physics letters **102**, p. 243101, 2013.

20. He, Xiaowei, Léonard, François , and Kono, Junichiro, "Uncooled Carbon Nanotube Photodetectors," Advanced Optical Materials, 3: 989–1011, 2015.

21. Janson, S.W., "Electric Propulsion for Low Earth Orbit Constellation Morphing," AIAA Paper 2002-3669, 38th AIAA/ASME/SAE/ASEE Joint Propulsion Conference, July 7-10, 2002.

22. SPENVIS web page, European Space Agency, URL: https://www.spenvis.oma.be/

23. The Grün Interplanetary Flux Model web page, URL: https://www.spenvis.oma.be/help/background/metdeb/metdeb.html#METFLUX

24. Divine, N. and Gruen, R., "Modeling the Meteoroid Distributions in Interplanetary Space and Near-Earth," Proceedings of the First European Conference on Space Debris, Darmstadt, Germany, April, 1993.

25. Neish, Michael J., and Kiebe, Seishiro, "Hypervelocity Impact Damage for Kapton® Multi-Layered Insulation and Teflon Second-Surface Mirrors," Proceedings of the Third European Conference on Space Debris, Darmstadt, Germany. 19 - 21 March 2001.

26. NASA Preferred Reliability Practices, "Micrometeroid Protection," practice number PD-EC-1107, May 1996, URL: http://www.klabs.org/DEI/References/design_guidelines/environment_series/1107.pdf